

# Supporting Information

## Optically Thin Metallic Films for High-radiative-efficiency Plasmonics

Yi Yang,<sup>\*,†</sup> Bo Zhen,<sup>†,‡</sup> Chia Wei Hsu,<sup>¶</sup> Owen D. Miller,<sup>§</sup> John D. Joannopoulos,<sup>†</sup>  
and Marin Soljačić<sup>†</sup>

<sup>†</sup>*Research Laboratory of Electronics, Massachusetts Institute of Technology, Cambridge,  
Massachusetts 02139, USA*

<sup>‡</sup>*Physics Department and Solid State Institute, Technion, Haifa 320000, Israel*

<sup>¶</sup>*Department of Applied Physics, Yale University, New Haven, CT 06520, USA*

<sup>§</sup>*Department of Mathematics, Massachusetts Institute of Technology, Cambridge, MA  
02139, USA*

E-mail: [yiy@mit.edu](mailto:yiy@mit.edu)

# Supporting Information

## A. Numerical methods

Mode profiles and eigenfrequencies are obtained using finite-element simulations provided by COMSOL. The 2D axial symmetric computational cell contains the torus/cylinder scatterer and the multilayer underneath. Perfectly matched layers are placed in all  $(r, z)$  directions and are far enough from the scatterer to emulate homogeneous ambient space. Eigenfrequency analysis is used to obtain the eigenvalues and eigenmodes.

Scattering and absorption cross-sections are obtained using the 3D total-field-scattered-field (TFSF) simulation in Lumerical. A TFSF plane wave source is placed around the scatterer. A surface integral on the Poynting vector surrounding the scatterer is calculated to extract the scattering cross-section. A volume integral on the loss per volume inside the scatterer is calculated to extract the absorption cross-section.

Spontaneous emission simulation is also implemented via Lumerical. A dipole source is placed at various locations in the active layer. Surface integrals of the Poynting vectors surrounding the dipole source and surrounding the nanoantenna are calculated to obtain the total and radiative (photon + plasmon) decay rates, respectively. The absorption decay rate is their difference. We note that the calculation of enhancement is implemented via directly probing the local density of states from a local dipole. The method does not rely on any low-loss or single-mode approximation.

To separate the decay rates of free space radiation ( $\Gamma_{\text{far}}$ ) and surface plasmon ( $\Gamma_{\text{SPP}}$ ) for both scattering (using the Mie plasmon) and emission (using the gap plasmon) simulations, multiple surface integrals of the Poynting vector are calculated surrounding the scatterer/emitter with different distance  $d$  from the scatterer/emitter ( $d$  varies from tens of nm to several  $\lambda$ ). As launched surface plasmon decays with increasing  $d$  while free space radiation does not, the integrated Poynting flux  $P$  can be accurately modelled as  $P(d) = Ae^{-Cd} + B$ , where  $A$  and  $B$  correspond to  $\Gamma_{\text{SPP}}$  and  $\Gamma_{\text{far}}$  respectively.

## B. Mode overlap

The normalization condition is

$$\int \varepsilon \mathbf{E}^2 d^3 \mathbf{r} = 1, \quad (\text{S1})$$

given the modes are non-Hermitian. The overlap of two modes  $\rho$  is calculated as<sup>1</sup>

$$\rho = \frac{\| \hat{\mathbf{z}} \cdot \int (\mathbf{E}_1 \times \mathbf{H}_2 + \mathbf{E}_2 \times \mathbf{H}_1) d^3 \mathbf{r} \|^2}{\| \hat{\mathbf{z}} \cdot \int \mathbf{E}_1 \times \mathbf{H}_1 d^3 \mathbf{r} \| \cdot \| \hat{\mathbf{z}} \cdot \int \mathbf{E}_2 \times \mathbf{H}_2 d^3 \mathbf{r} \|}, \quad (\text{S2})$$

where  $\hat{\mathbf{z}}$  is the direction of propagation.

Here we adopt the unconjugated cross product because of the non-Hermiticity, although the conjugated product will also work in this case, since the relevant field components are mostly real. We note that  $\rho$  also has alternate definitions.<sup>2</sup> Both definitions produce the same curves shown in Fig.3.

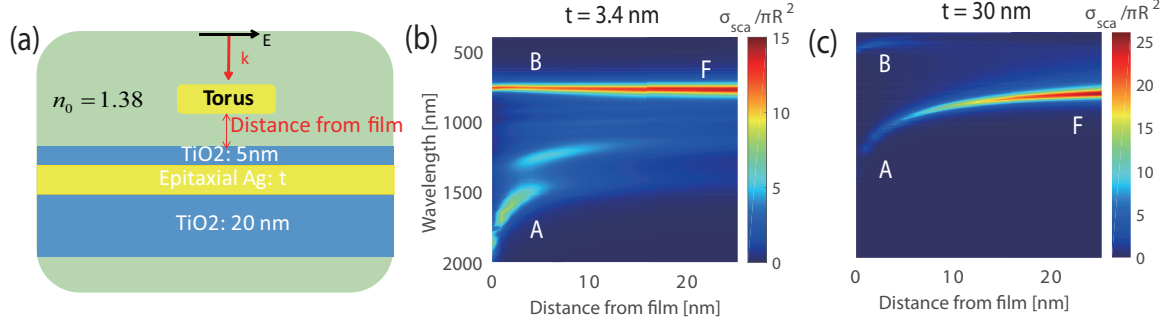


Figure S1: (a) Schematic illustration of the scattering of a silver torus with different particle-multifilm distance. Evolution of  $\sigma_{\text{sca}}$  when the metallic layer is optically (b) thin or (c) thick. A and B denote the gap and torus plasmon resonances of the composite structure, respectively. F denotes the Mie resonance of the torus in free space. When the torus is far away from the film, the near field interaction between the two is weak. As shown from the right of (b) and (c), both the thin-film and thick-film case demonstrate the Mie plasmon resonance as in free space, denoted by  $F$ . When the torus approaches the metallic multifilm, however, the evolution of  $\sigma_{\text{sca}}$  becomes very different. For the thin-film case,  $F$  converges to  $B$  with a stable resonant wavelength and narrowed linewidth. For the thick-film case,  $F$  converges to  $A$  with redshifting resonant wavelength and decreasing  $\sigma_{\text{sca}}$ . We also note that the gap plasmon resonance split into two branches for the thin-film case due to the coupling of two surface plasmons in the metal-insulator-metal-insulator structure.<sup>3</sup>

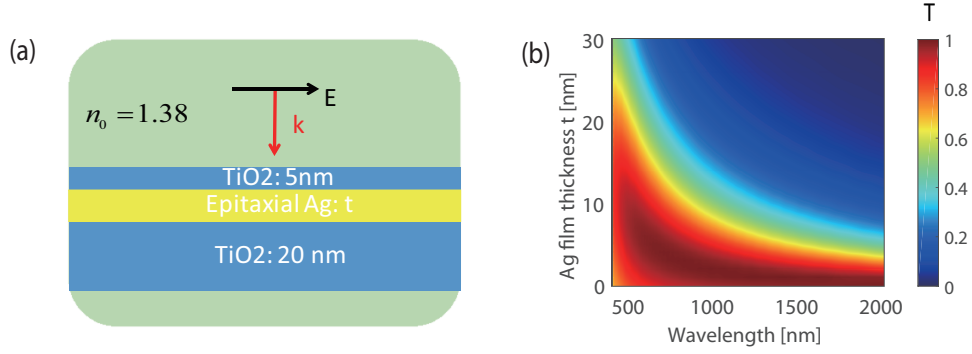


Figure S2: (a) Schematic illustration of the  $\text{TiO}_2\text{-Ag-TiO}_2$  multilayer. (b) Transmission at normal incidence as a function of silver film thickness. Broadband high transmission is shown when the thickness of silver film is less than 10 nm.

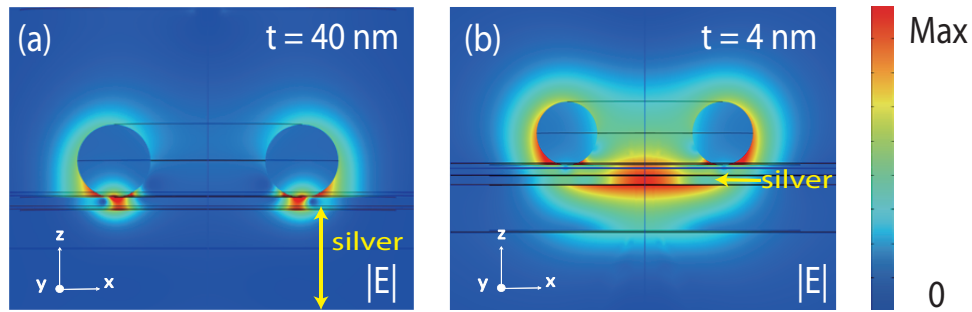


Figure S3: A better mode squeezing into the silver film (thickness denoted by  $t$ ) is realized when the silver film is optically thin, as can be seen by comparing the  $|E|$  field of the film-coupled Mie resonance when (a)  $t = 40$  nm and (b)  $t = 4$  nm. The yellow arrow indicates the silver film in the multilayer.

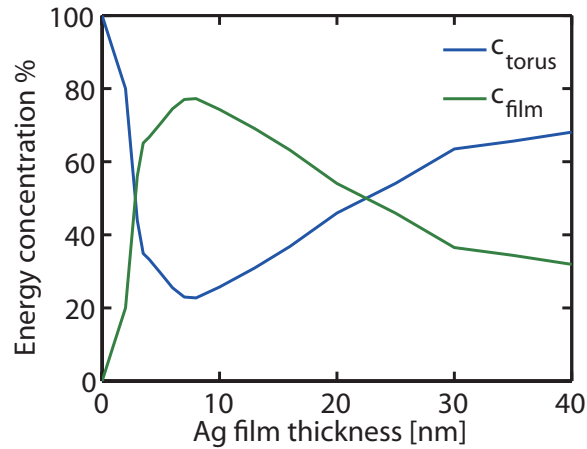


Figure S4: Energy concentration coefficients as a function of silver film thickness. The highest concentration in the film happens when the the film is optically thin.

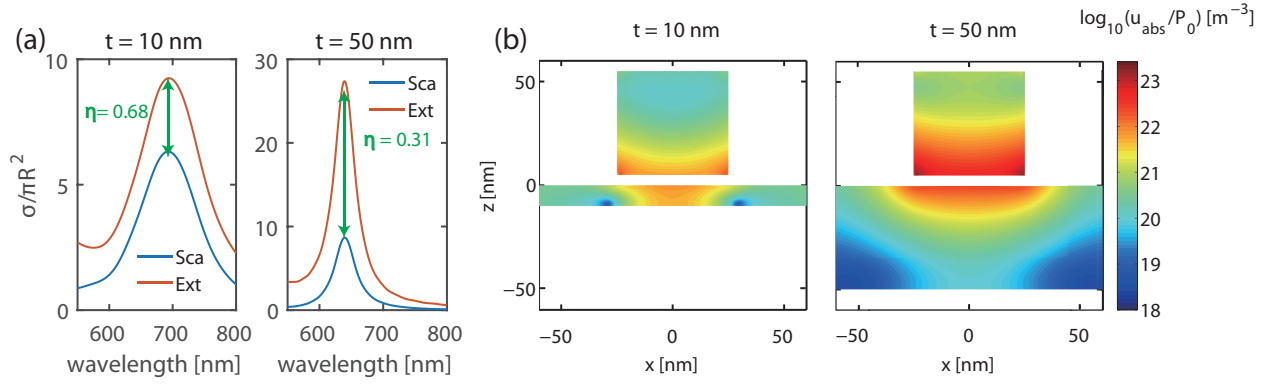


Figure S5: (a) Scattering and extinction cross-sections of the cylinder and (b) normalized absorption per unit volume at normal incidence with different silver film thicknesses (left:  $t = 10$  nm; right:  $t = 50$  nm). The scattering cross-sections of the two cases are about the same, yet along with a six-fold enhancement of absorption for the  $t = 50$  case. Correspondingly, the radiative efficiency  $\eta$  drops by half. The efficiency contrast is also implied from the absorption per unit volume, which is greatly reduced inside the film as well as inside the cylinder by reducing the thickness of the metallic layer.

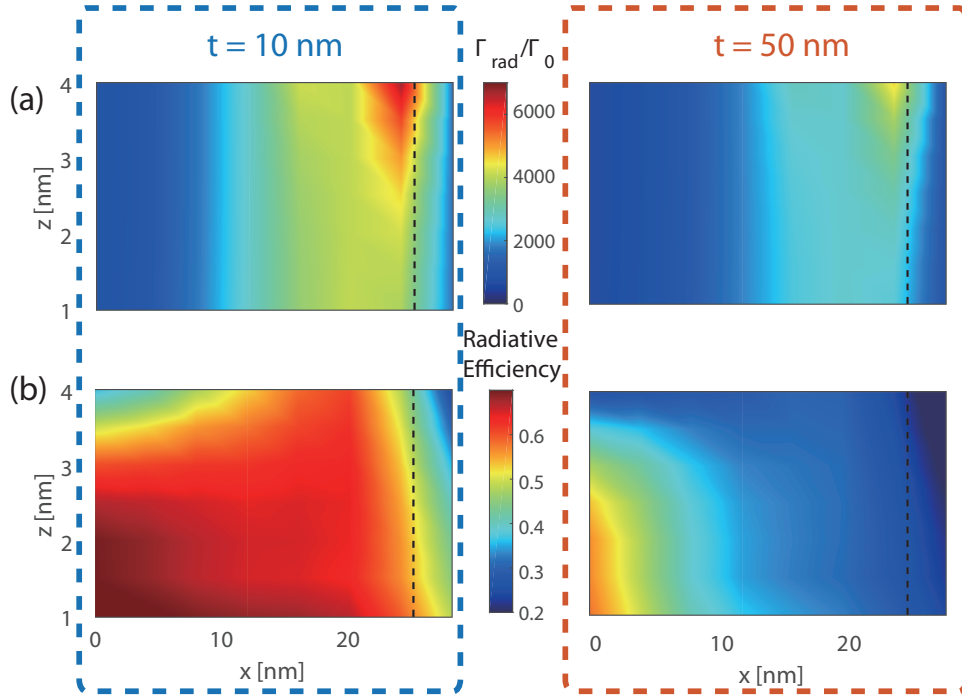


Figure S6: Spontaneous emission enhancement using the epitaxial silver film [instead of the Palik silver film while other configurations are the same as those in Fig.4(c)(d)]. A higher radiative efficiency can be achieved. (a) Normalized radiative decay rate and (b) Quantum efficiency as a function of dipole location in the  $x - z$  plane (left:  $t = 10$  nm; right:  $t = 50$  nm).

## References

- (1) Johnson, S. G.; Bienstman, P.; Skorobogatiy, M.; Ibanescu, M.; Lidorikis, E.; Joannopoulos, J. *Phys. Rev. E* **2002**, *66*, 066608.
- (2) Palamaru, M.; Lalanne, P. *Appl. Phys. Lett.* **2001**, *78*, 1466–1468.
- (3) Economou, E. N. *Phys. Rev.* **1969**, *182*, 539.